Human Poly (ADP-ribose) Polymerase Family Member 14 (PARP14)

A Target Enabling Package (TEP)

We respectfully request that this document is cited using the DOI value as given above if the content is used in your work.

USEFUL LINKS

(Please note that the inclusion of links to external sites should not be taken as an endorsement of that site by the SGC in any way)

SUMMARY OF PROJECT

This work provides reagents to develop specific inhibitors of the macrodomains of PARP14, for potential use for cancer and/or inflammation. Targeting the macrodomains of PARP14 is an alternative targeting strategy to PARP catalytic domain inhibitors that may allow greater inhibitor selectivity, and an alternative cellular effect.

This package includes protein purification protocols, crystal structures of the 2nd and 3rd macrodomain of PARP14 in complex with small molecule chemical starting points, *in vitro* assays to measure ligand binding

to the macrodomains, as well as validation of a PARP14 antibody and reagents to generate PARP14 knock-out cell lines (CRISPR-Cas9).

SCIENTIFIC BACKGROUND

There are at least 17 PARP enzymes in the human genome most of which can either mono- or poly-ADP-ribosylate their substrates [1,2]. PARPs are the writers of the ADP-ribose post-translational modification. One of the several evolutionary conserved readers of ADP-ribosylation are the macrodomains. PARP14 is a large gene with multiple interaction domains including RRM (RNA recognition motif) domains, three macrodomains, a WWE domain and a C-terminal PARP domain. PARP14 therefore contains multiple reader domains and a writer domain for mono-ADP-ribosylation. PARP14 is also known as BAL2, B aggressive lymphoma protein 2.
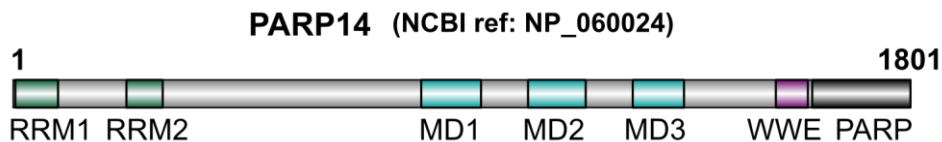
PARP14 was identified as a co-activator of STAT6 that enhances STAT6-mediated gene transcription in response to IL-4 [3,4]. PARP14 assists the release of HDAC2 and HDAC3 from promoters, freeing the promoters for STAT6 binding [5]. IL-4/STAT6 signalling is important both for the development of T cells into differentiated subtypes and for the stimulation of B cells. As a consequence there are links between PARP14 and lymphomagenesis and with immune system regulation.

In B cells, in response to IL-4, PARP14 induces pro-survival factors [6], and is a promoter of B-lymphoid oncogenesis [7]. PARP14 suppresses the expression of the pro-apoptotic kinase JNK1, and in myeloma cells PARP14 overexpression prevented apoptosis induced by JNK2 knockdown [8]; myeloma cells were found to have high expression of PARP14, which was associated with poor survival. PARP14 is also highly expressed in many solid tumours, especially HCC, and is a poor prognosis marker in Renal Clear Cell Carcinoma [9,10]. A rare PARP14-TFE3 translocation has also been found in RCC, involving the first two exons of PARP14 [11].

For inflammatory disease, it was shown that PARP14$^{-/-}$ mice are healthy, but showed reduced IgE and lung pathology in an allergic airway disease model [12]. The data suggested that PARP14 promoted Th2 differentiation and allergic airway disease [12]. PARP14$^{-/-}$ mice have reduced Th17 differentiation and Tfh development, an effect that was also seen with PARP inhibitors [13]. It is also notable that PARP14 is a component of stress granules [14]. Overall the data suggests PARP14 as a target for allergic asthma as well as allergic airway disease [12,15], and generally in allergic inflammation [16–18].

There have been several recent efforts to find inhibitors of the PARP14 PARP domain [19–21]. The study of Peng *et al.* [19] was interesting for showing that in principle PARP14 chemical inhibition (of its catalytic domain) in HepG2 cells could show a similar effect on JNK1 phosphorylation and PARP1 cleavage as PARP14 knock-down by siRNA.

Better PARP14 PARP domain inhibitors could be effective, but it may require synthesising inhibitors that are selective over the other 17-18 PARPs. An alternative strategy would be to inhibit localisation of PARP14 to respective target sites via inhibition of its macrodomains. Due to the low homology of PARP macrodomains to other human macrodomains, and the relatively low affinity of PARP macrodomains for ADP-ribose, this offers a route to specific PARP14 modulators.

Proteins purified: PARP14 Macrodomains 1, 2, and 3

We have expressed and purified the following constructs of human PARP14, all in *E. coli*:

Construct ID	Residue range	Domain	Tag
PARP14A-c028	Gly789 – Lys979	PARP14 MD1	N-terminal His$_6$
PARP14A-c001	Ser794 – Asp984	PARP14 MD1	N-terminal His$_6$, C-terminal AVI (for biotinylation)
PARP14A-c030	Ala994 – Asn1191	PARP14 MD2	N-terminal His$_6$
PARP14A-c002	Ala994 – Asn1191	PARP14 MD2	N-terminal His$_6$, C-terminal AVI (for biotinylation)
PARP14A-c032	Phe1208 – Gly1388	PARP14 MD3	N-terminal His$_6$
PARP14A-c003	Phe1208 – Gly1388	PARP14 MD3	N-terminal His$_6$, C-terminal AVI (for biotinylation)
A construct of the PARP domain was published in Wahlberg *et al.* [22].		PARP	N-terminal His$_6$

Structures

PARP14 MD2 and MD3 were previously crystallised bound to ADP-ribose. We have established crystallisation systems for PARP14 MD2 and MD3 bound to inhibitors, giving high-resolution diffraction in both cases.

PARP14 MD2
The wild-type PARP14 MD2 sequence failed to yield a co-crystal structure with inhibitors from the GeA-69 series, so a set of surface-entropy-reduction (SER) mutant constructs were created as below. One of these constructs (PARP14A-c013) generated a 1.6 Å resolution structure bound to MnK2-13, the sulfonamide analogue of GeA-69(PDB ID 5O2D). Superimposition of the PARP14 MD2–MnK2-13 co-crystal structure with the ADP-ribose bound structure (PDB ID 3Q71) revealed an allosteric binding mode of the GeA-69 series to this domain.

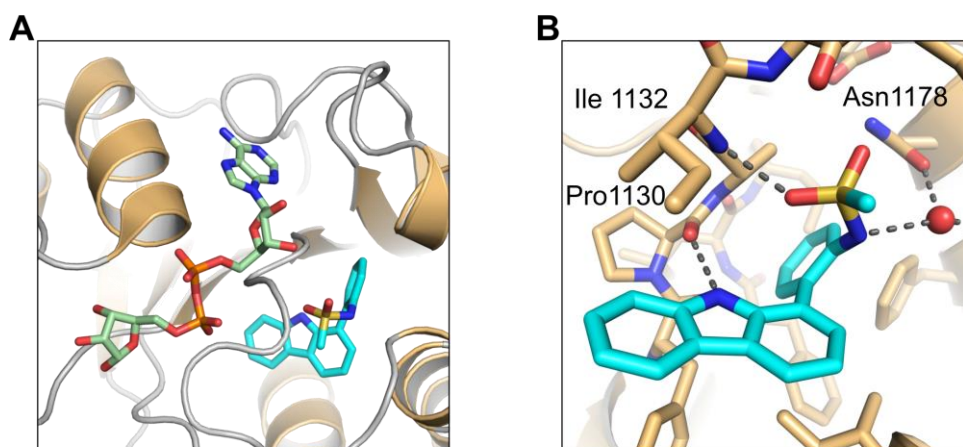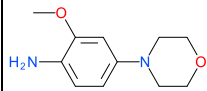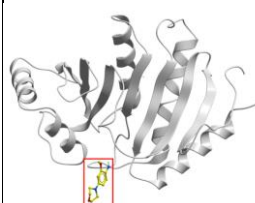| Construct ID	Residue range	Mutation	Tag
PARP14A-c011	Ala994 – Asn1191	p.K1048S, p.K1106S, p.K1154S, p.K1158S, p.K1162S	N-terminal His$_6$
PARP14A-c013	Ala994 – Asn1191	p.K1048S, p.K1154S, p.K1158S, p.K1162S	N-terminal His$_6$
PARP14A-c014	Ala994 – Asn1191	p.K1106S, p.K1154S, p.K1158S, p.K1162S	N-terminal His$_6$
PARP14A-c015	Ala994 – Asn1191	p.K1048S	N-terminal His$_6$
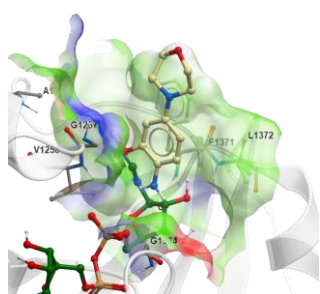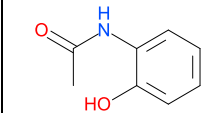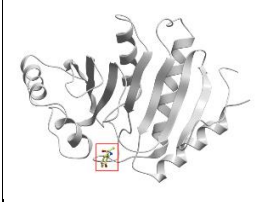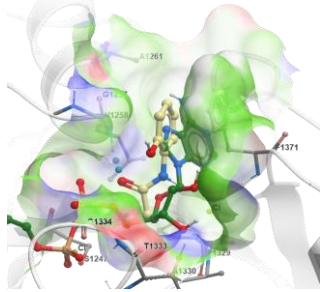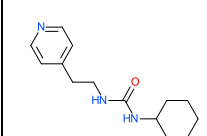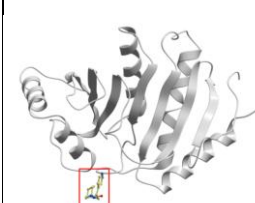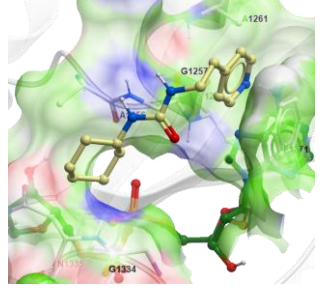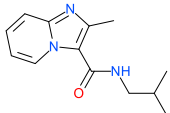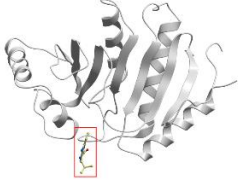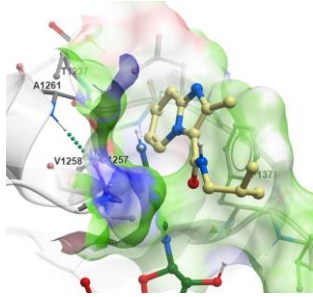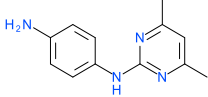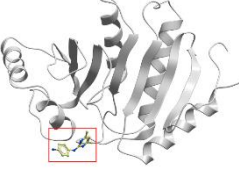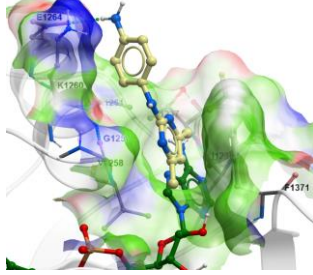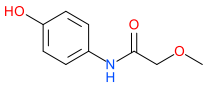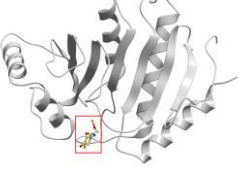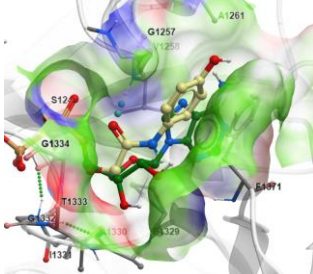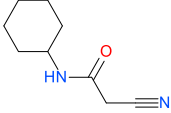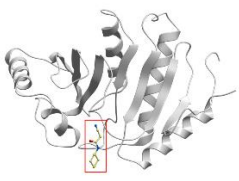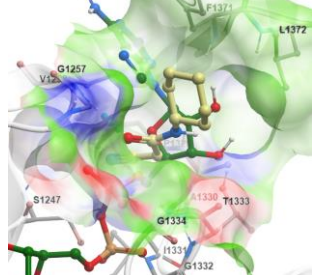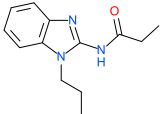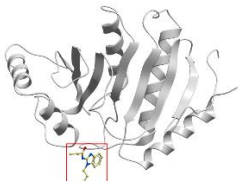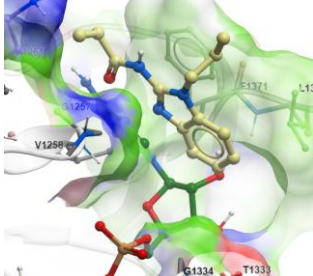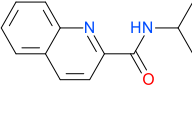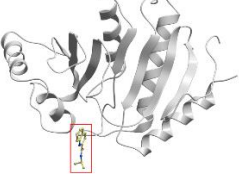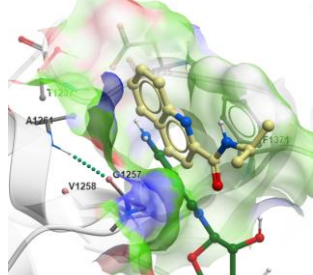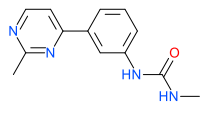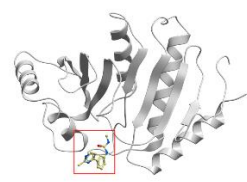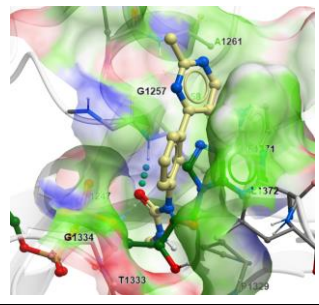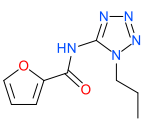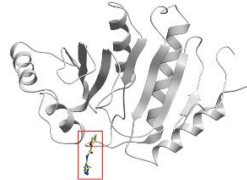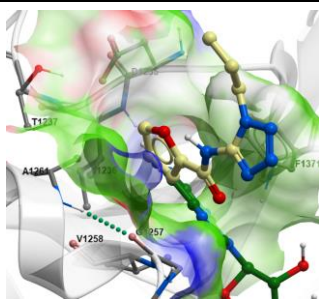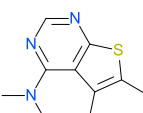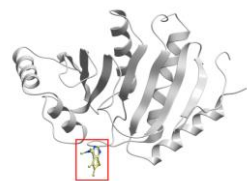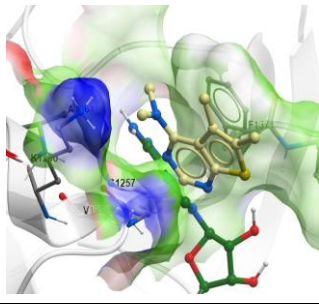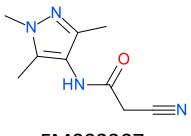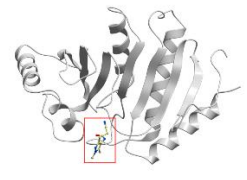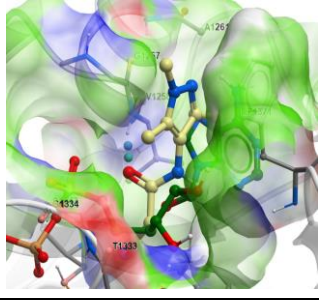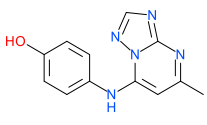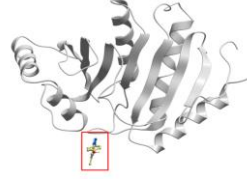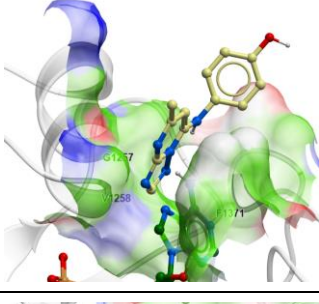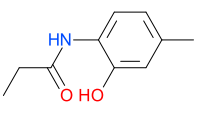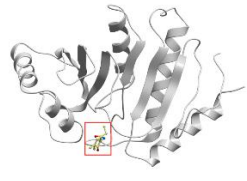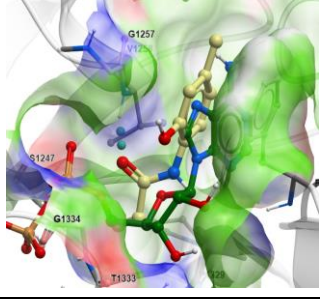
Figure 1. (A) Overlay of bound ADP-ribose (Green sticks) (PDB ID 3Q71) superimposed with PARP14 MD2 (brown sheets and helices, grey loops) in complex with MnK2-13 (cyan sticks) structure (PDB ID 5O2D). **(B)** H-Bonding displayed in co-crystal structure of PARP14 MD2 (brown sticks) and MnK2-13 (cyan sticks) structure (PDB ID 5O2D).
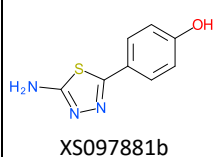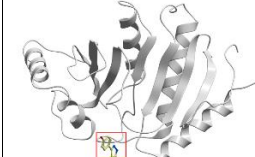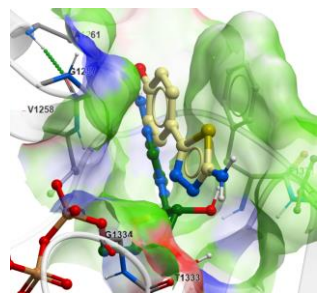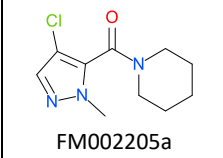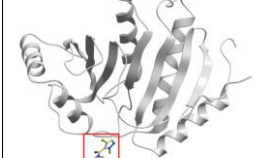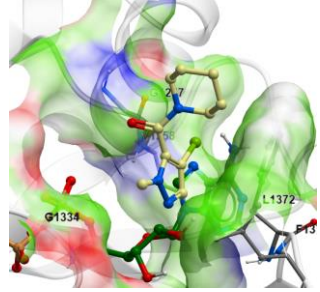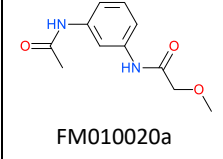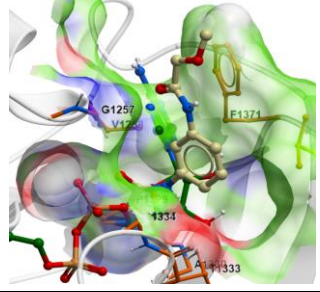
PARP14 MD3

The PARP14 MD3 construct PARP14A-c032 was used for crystallisation of this domain. Optimisation of experimental conditions gave a reliable crystallisation system suitable for soaking inhibitors, which routinely generated high-resolution co-crystal structures. A fragment screen by X-ray crystallography generated the following chemical starting points for PARP14 MD3.

PDBID	Ligand/ Compound ID	Binding Location	Binding pocket	Resolution (Å)
5QHT	FM010005a			1.1
5QHU	FM001707a			1.1
5QHV	FM001999a			1.1

5QHW	XS106503b			1.1
5QHX	FM001875a			1.1
5QHY	FM001884a			1.1
5QHZ	FM010067a			1.1
5QI0	FM002036a			1.1
5QI1	FM002044a			1.1

5QI2	FM001702a			1.1
5QI3	FM001958a			1.1
5QI4	FM001909a			1.2
5QI5	FM002207a			1.1
5QI6	FM001942a			1.1
5QI7	FM002062a			1.1

For more information regarding any aspect of TEPs and the TEP programme, please contact teps@thesgc.org

5QI8	XS097881b			1.1
5QI9	FM002205a			1.1
5QIA	FM010020a			1.1

The doi for the electron density map analysis is: 10.5281/zenodo.1247822

IMPORTANT: Please note that the existence of small molecules within this TEP only indicates that chemical matter can bind to the protein in a functionally relevant pocket. As such, these molecules should not be used as tools for functional studies of the protein unless otherwise stated as they are not sufficiently potent or well-characterised to be used in cellular studies. The small molecule ligands are intended to be used as the basis for future chemistry optimisation to increase potency and selectivity and yield a chemical probe or lead series.

Assays

AlphaScreen

We developed an AlphaScreen-based assay using a peptide that is biotinylated and ADP-ribosylated. For MD2 the optimal concentrations of protein and peptide were 400 nM and 25 nM, and for MD3 the optimal concentrations were 200 nM and 50 nM. With these concentrations good assay performance was observed.
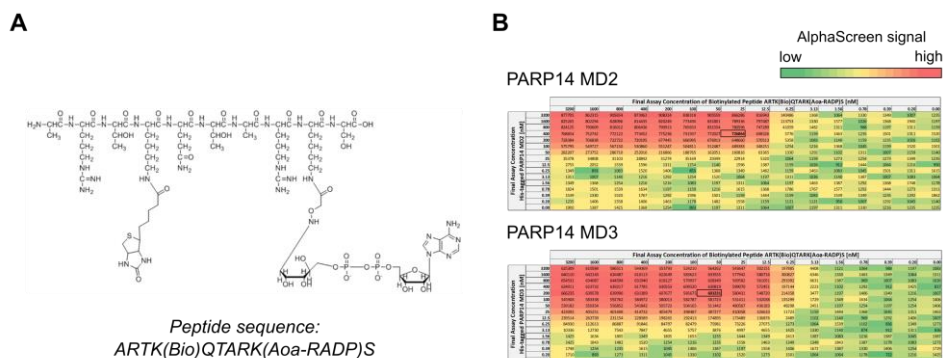
Figure 2. (A) Molecular structure of the biotinylated and ADP-ribosylated 11 residue peptide designed for macrodomain screening by AlphaScreen. **(B)** Dose-response titration results of PARP14 MD2 and MD3 and the macrodomain AlphaScreen peptide shown in **(A)** for determining the optimal assay concentrations of protein and peptide.
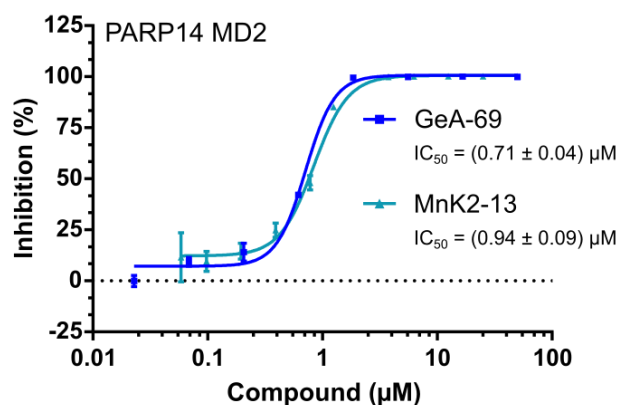
Figure 3. GeA-69 and MnK2-13 IC_{50} determination for PARP14 MD2 by AlphaScreen.

Biolayer Interferometry (BLI) measurement of inhibitor binding

The biotinylated proteins available using the expression systems above enable binding of PARP14 MD2 or MD3 to streptavidin-coated surfaces, for use in techniques such as Biolayer Interferometry (BLI) or Surface Plasmon Resonance (SPR).
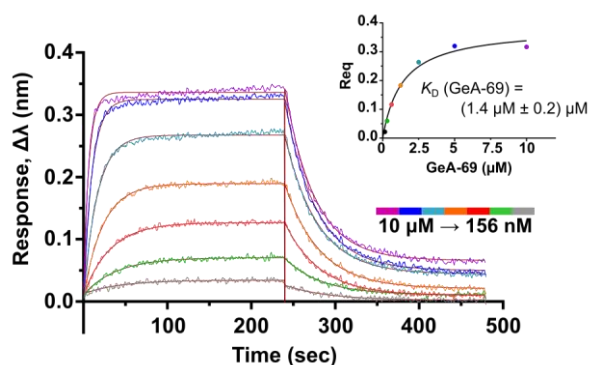
Figure 4. Determination of binding kinetics of GeA-69 to PARP14 MD2 by Biolayer Interferometry (BLI).

Isothermal Titration Calorimetry (ITC)

It was possible to measure binding of MD2 to nucleotides (with ligand in the syringe) or to inhibitors (with ligand in the cell).
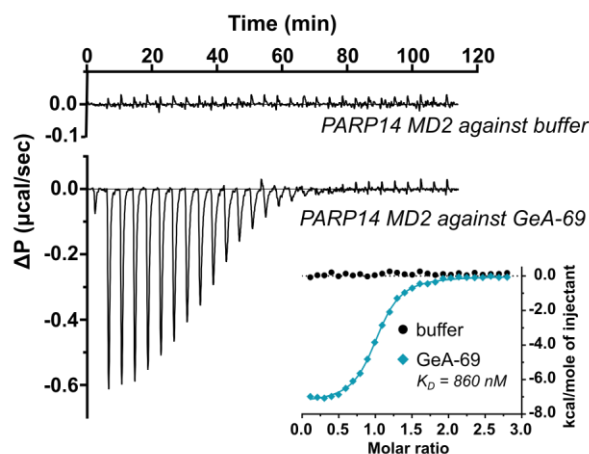
Figure 5. Example of measuring the thermodynamic binding profile of GeA-69 to PARP14 MD2 by Isothermal Titration Calorimetry (ITC). Raw injection heats are shown, with the data fitting to a binding isotherm (one site binding model) in the inset.

Seventeen molecules were identified binding to PARP14 MD3 in the fragment screen (shown above). The carbazole-based molecule GeA-69 was identified as an allosteric inhibitor of PARP14 MD2 ADP-ribose binding by library screening using the above-mentioned AlphaScreen assay.

A limited SAR exploration of the carbazole-based inhibitors of PARP14 MD2 was performed with ~110 compounds synthesised and screened in collaboration with the groups of Prof. Dr. Franz Bracher (Department Pharmazie, Zentrum für Pharmaforschung, Ludwig-Maximilians-Universität, München) and Prof. Paul Brennan (SGC, Oxford); this data was published in Bioorg. Med. Chem. (2018) [23].
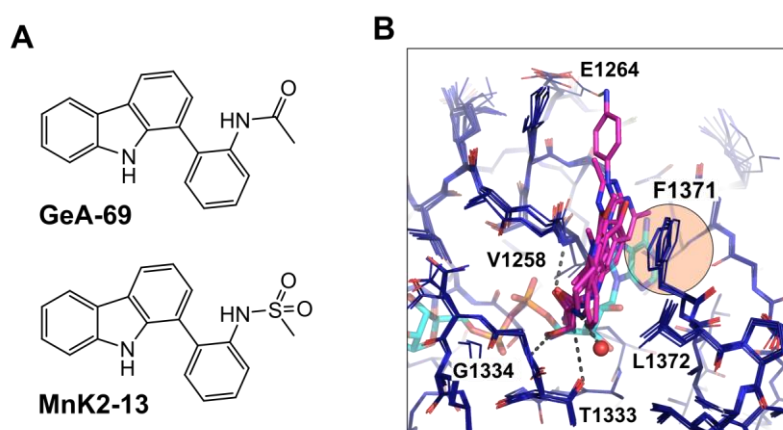
Figure 6. Chemical matter for PARP14 MD2 and MD3. **(A)** Molecular structure of GeA-69 and MnK2-13 targeting PARP14 MD2. **(B)** Superimposed fragments targeting the ADP-ribose binding site of PARP14 MD3. As reference for the position of the fragments, PARP14 MD3 in complex with ADP-ribose (PDB ID 4ABK) [24] was superimposed with the corresponding fragment structure and the ADP-ribose shown as atom-coloured sticks in low transparency in the model. Phe1371 is targeted by all fragments.

PARP14 Antibody

A commercially available monoclonal mouse PARP14 antibody C-1 (Santa Cruz Biotechnology, sc-377150) was validated by Western blot.
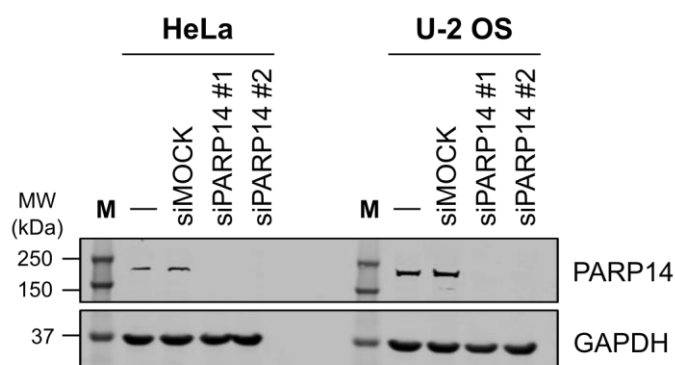
Figure 7. Testing PARP14 expression and knock-down in HeLa and U-2 OS cells by Western Blotting. The PARP14 antibody was used 1:750 in 5 % milk/TBS-T. Details of the PARP14 targeting siRNAs #1 and #2 are in Nicolae *et al.* [25].

CRISPR reagents

We designed the following reagents which were successfully used to knock-out PARP14 in HeLa and U-2 OS cells.

Plasmids for PARP14 gene editing using the CRISPR-Cas9 system			
Construct ID	**PARP14 target sequence (fwd, 5' → 3')**	**Cas9 type**	**Vector**
pSpCas9(BB)-2A-Puro-PARP14-c002	CGGCGAGTGTGAGGTCCGCC	wild-type	pSpCas9(BB)-2A-Puro (addgene #48139)
pSpCas9(BB)-2A-Puro-PARP14-c004	TCAAGTTCTTCGGGGGGGTCG	wild-type	pSpCas9(BB)-2A-Puro (addgene #48139)
pSpCas9n(BB)-2A-Puro-PARP14-c001	CTCCCGACCTCTTCGGGCTC	nickase	pSpCas9n(BB)-2A-Puro v2.0 (addgene #62987)
pSpCas9n(BB)-2A-Puro-PARP14-c003	CGGCGAGTGTGAGGTCCGCC	nickase	pSpCas9n(BB)-2A-Puro v2.0 (addgene #62987)
pSpCas9n(BB)-2A-Puro-PARP14-c005	TCAAGTTCTTCGGGGGGGTCG	nickase	pSpCas9n(BB)-2A-Puro v2.0 (addgene #62987)
pSpCas9n(BB)-2A-Puro-PARP14-c006	TGTACTTCCAGAGCCCGAAG	nickase	pSpCas9n(BB)-2A-Puro v2.0 (addgene #62987)
Note: sgRNAs target the exon 1 of PARP14 on chromosome 3, transcript ENST00000474629.			
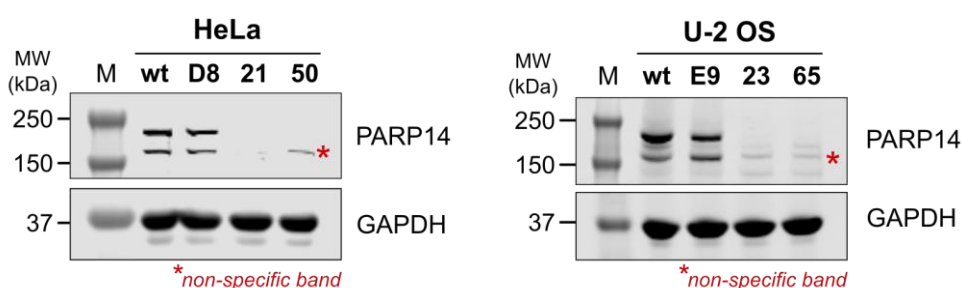
Figure 8. Generation of PARP14 knock-out HeLa and U-2 OS cell lines by CRISPR-Cas9 using the above-mentioned sgRNAs. (wt = heterogeneous parental cell line; D8 and E9 = clonal wild-type cell lines generated with GFP-targeting sgRNAs; PARP14 was knocked-out in the HeLa clones 21, 50 and the U-2 OS clone 23 using the sgRNA combination pSpCas9n(BB)-2A-Puro-PARP14-c001 and -c003 while the U-2 OS clone 65 was derived by transfection with sgRNA pSpCas9(BB)-2A-Puro-PARP14-c002.)

There are also commercially available reagents for generating PARP14 knockout cell lines from Santa Cruz Biotechnology (Cat. # sc-402812) and BioCat (Cat. # KN220878-OR). We have not tested these reagents.

Publications

The inhibitor of PARP14 MD2 (GeA-69) and the crystal structure of PARP14 MD2 with the related compound MnK2-13 have been published [26]. Some initial structure-activity relationship data for the development of GeA-69 has also been published [23].

Future Plans

An examination of the role of PARP14 in the response to replication stress and DNA damage is in progress.

CONCLUSION

The protein materials, assay protocols and initial chemical matter provide a starting point for evaluating the alternative strategy of targeting PARP14 macrodomains, for potential use in cancer or allergic inflammation.

FUNDING INFORMATION

For more information regarding any aspect of TEPs and the TEP programme, please contact teps@thesgc.org

Structure Files

PDB ID	Structure Details	Fragment Supplier
5O2D	PARP14 macrodomain 2 with ligand MnK2-13	
5QHT	PARP14 macrodomain 3 with fragment N13417a	Key Organics
5QHU	PARP14 macrodomain 3 with fragment N08149b	Alfa Aeasar
5QHV	PARP14 macrodomain 3 with fragment N13681a	Asinex
5QHW	PARP14 macrodomain 3 with fragment N13729a	ChemBridge
5QI0	PARP14 macrodomain 3 with fragment N13734a	Apollo Scientific
5QI1	PARP14 macrodomain 3 with fragment N13856a	Enamine
5QI6	PARP14 macrodomain 3 with fragment N13979a	Crea-Chim UAB
5QI3	PARP14 macrodomain 3 with fragment N13857a	ChemBridge
5QI4	PARP14 macrodomain 3 with fragment N13848a	Enamine
5QI8	PARP14 macrodomain 3 with fragment N13987a	Maybridge
5QI9	PARP14 macrodomain 3 with fragment N14095a	Enamine
5QHX	PARP14 macrodomain 3 with fragment N13660a	Enamine
5QHY	PARP14 macrodomain 3 with fragment N13844a	Maybridge
5QHZ	PARP14 macrodomain 3 with fragment N13767a	IBScreen
5QI2	PARP14 macrodomain 3 with fragment N13462a	Enamine
5QI5	PARP14 macrodomain 3 with fragment N14015a	IBScreen
5QI7	PARP14 macrodomain 3 with fragment N13888a	Specs
5QIA	PARP14 macrodomain 3 with fragment N13605a	Crea-Chim UAB

Materials and Methods

Protein expression and purification

Macrodomain proteins (PARP14 MD1, MD2, MD2$_{SERmut}$ and MD3) were expressed using constructs that add tobacco etch virus (TEV) protease-cleavable His$_6$-tags. Transformed BL21(DE3)-R3-pRARE cells were grown at 37 °C in LB medium (Miller) supplemented with appropriate antibiotics until OD$_{600}$ reached 0.5–0.6, then cooled to 18 °C and supplemented with 0.5 mM isopropyl β-D-1-thiogalactopyranoside (IPTG) at an OD$_{600}$ of 0.8 to induce protein expression overnight. For purification of *in vivo* biotinylated macrodomain proteins, the constructs were transformed into BL21(DE3)-R3-BirA cell line (BL21 derivative coexpressing BirA using a pACYC coexpression vector). Cells were grown at 37 °C in LB medium (Miller) until OD$_{600}$ reached 0.5–0.6, then cooled to 18 °C and supplemented with 0.5 mM D-biotin dissolved in 10 mM bicine (pH 8.3) and 0.5 mM IPTG at an OD$_{600}$ of 0.8 to induce protein expression overnight. Cell pellets re-suspended in lysis buffer (50 mM HEPES (pH 7.4), 500 mM NaCl, 20 mM imidazole, 5 % glycerol, 0.5 mM tris(2-carboxyethyl)phosphine [TCEP], 1:2,000 Calbiochem protease inhibitor cocktail set III) were quickly thawed on ice and lysed by high pressure homogenisation. Following cell lysis, DNA was precipitated with 0.15 % polyethyleneimine (PEI) and insoluble cell debris was removed by centrifugation (36000×g, 1 h, 4 °C). His6- (-biotin) tagged proteins were purified using Ni-Sepharose resin (GE Healthcare) and eluted stepwise in binding buffer with 40–250 mM imidazole. A high salt wash with 1 M NaCl was combined with the first elution step including 40 mM imidazole. As required, the His$_6$-tag was removed from the macrodomain proteins at 4 °C overnight using recombinant TEV protease (used 1:40 -1:100 *(w/w)*) before gel filtration (Superdex 75 16/60, GE Healthcare) in GF buffer (25 mM HEPES (pH 7.4), 300 mM NaCl, 5 % glycerol, 0.5 mM TCEP). Proteins with removed His$_6$- tag were additionally passed over Ni-Sepharose resin as a final purification step. In the case of PARP14 MD2 and MD3 purification for crystallisation, TEV His$_6$-tag cleavage after the first Ni-IMAC purification step was combined with overnight dialysis using SnakeSkin® Dialysis Tubing, 3500 MWCO (Thermo Scientific). The dialysed sample was passed over Ni-Sepharose resin before purification by gel filtration (Superdex 75 16/60) and further purification steps. For PARP14 MD3 the GF buffer contained 20 mM HEPES (pH 7.4), 300 mM NaCl, 10 % glycerol and 0.5 mM TCEP. Apart from Ni-IMAC rebinding, all purification steps were carried out at 4 °C.

AlphaScreen assay

Assays were performed with minor modifications from the manufacturer's protocol (PerkinElmer) [27,28]. All reagents were diluted in buffer containing 25 mM HEPES (pH 7.4), 100 mM NaCl, 0.5 mM TCEP, 0.1 % BSA and 0.05 % CHAPS and allowed to equilibrate to RT before addition to plates. The assays were run in 20 µL volumes in low-volume 384-well plates (ProxiPlate™-384 Plus, PerkinElmer) at RT. To determine ideal assay concentrations of the corresponding macrodomain protein and the macrodomain AlphaScreen peptide (a biotinylated and ADP-ribosylated 11 residue sequence), 4 µL volumes of peptide (0-16 µM; final assay concentration: 0-3.2 µM) were incubated with 4 µL volumes of His_6-tagged macrodomain protein (0-16 µM; final assay concentration: 0-3.2 µM) in 4 µL buffer for 30 min at RT in foil-sealed plates. For compound screening and IC_{50} characterisation, 12 µL of a solution containing peptide and His_6-tagged macrodomain protein in the pre-determined assay concentrations in assay buffer were incubated for 30 min at RT with 50 nL or 100 nL compound solution (pre-dispensed into the assay plate from 10 mM or 50 mM DMSO stocks using an Echo 550 (Labcyte)). Then, 8 µL of streptavidin-coated donor beads (7 µg/ml) and nickel chelate acceptor beads (7 µg/ml) (Perkin Elmer AlphaScreen™ Histidine (Nickel Chelate) Detection Kit) were added under low light conditions and plates were incubated for 60 min at RT protected from light. Plates were read on a PHERAstar FS plate reader (BMG Labtech) using an AlphaScreen 680 excitation/570 emission filter set. Alternatively for counterscreening of the compounds, 12 µL of 75 nM biotinylated and His_6-tagged linker peptide (PerkinElmer) was added to 50 nL or 100 nL of the compounds and plates were processed as described above.

Biolayer Inteferometry

Kinetic ligand-binding measurements were performed using an Octet RED384 BLI instrument (fortéBio) [29]. Superstreptavidin (SSA) biosensors were loaded with biotinylated macrodomain protein and equilibrated for 120 sec in assay buffer (25 mM HEPES (pH 7.4), 100 mM NaCl, 0.01 % Tween 20). Association and dissociation were monitored for 240 sec each in assay buffer at 25 °C. For compound characterisation, compounds were typically prepared as seven 1:1 serial dilutions starting from 10 µM or 50 µM. Binding to the reference sensors (no protein attached) was subtracted before calculations and data was processed using the fortéBio analysis software provided by the manufacturer.

Crystallisation of PARP14 MD2 with MnK2-13

Surface entropy reduction (SER) mutations were introduced into PARP14 MD2 (A994–N1191) by the overlapping PCR method. Several mutants were prepared, of which construct PARP14A-c013 with K1048S, K1154S, K1158S, and K1162S mutation could be crystallized with MnK2-13. For protein crystallization, purified PARP14A-c013 was buffer exchanged into 20 mM HEPES (pH 7.4), 500 mM NaCl, 5% glycerol, and 0.5 mM TCEP, and concentrated to 16 mg/mL, using 10 kDa MWCO centrifugal concentrators (Millipore). MnK2-13 inhibitor dissolved to 50 mM in DMSO was added to a final concentration of 1.0 mM (2 % DMSO) and incubated on ice for approximately 30 min. The sample was centrifuged at 14,000 rpm for 10 min at 4 °C prior to setting up 150 nL volume sitting drops at three ratios (2:1, 1:1, or 1:2 protein–inhibitor complex to crystallization solution). A crystal was obtained with a 1:2 ratio of protein to a crystallization solution consisting of 0.8 M sodium phosphate monobasic, 0.8 M potassium phosphate dibasic, and 0.1 M HEPES at pH 7.5 and was cryoprotected in mother liquor supplemented with 25 % ethylene glycol before flash-freezing in liquid nitrogen for data collection. Diffraction data were collected at the Diamond Light Source (Harwell, UK) beamline I02.

Crystallisation of PARP14 MD3 with fragments

PARP14 MD3 *apo* was crystallised by mixing on pre-cooled sitting drop crystallisation plates 100 nL of 30 mg/mL protein in 20 mM HEPES (pH 7.4), 300 mM NaCl, 10 % glycerol, 0.5 mM TCEP with 50 nL of reservoir solution containing 80 mM KBr and 30 % PEG2000MME and adding 15 nL of a crystal seed solution obtained from a previous crystallisation experiment, diluted 1:500 from the stock in 90 mM KBr and 30 % PEG2000MME. The seeds were prepared from a single crystal growing in 90 mM KBr and 30 % PEG2000MME which was

smashed to seeds using a 3 mm PTFE seed bead (Fisher Scientific) using standard laboratory vortex at full speed in 100 µL reservoir solution. Crystal growth was completed after 24 hours with incubation at 4 °C. PARP14 MD3 *apo* crystals were soaked with compounds from the DSPL2.0 library consisting of 776 fragments at 500 mM in DMSO-d_6 (and a subset in ethylene glycol). Soaking was performed by acoustically transferring 17.5 nL of compound solution to the crystallisation drop using an Echo 550 (Labcyte) [30] resulting in a final compound concentration of 50 mM with 10 % DMSO, calculated based on the initial drop volume. Crystals were incubated for 4-6 hours at 4 °C and then harvested (without cryoprotection) and cryocooled before X-ray diffraction data collection on the beamline I04-1 at Diamond Light Source (Harwell, UK).

Coordinates and structure factors for all data sets are deposited in the RCSB Protein Data Bank. Data collection and refinement statistics are available from the PDB pages.

Structure determination

PARP14 MD2
The diffraction data collected from a PARP14 MD2-MnK2-13 co-crystal was processed using MOSFLM [31] and AIMLESS [32]. The structure was solved by molecular replacement using PHASER [33] and a published structure of PARP14 MD2 (PDB ID 3Q71) as a search model. There was one molecule of PARP14 MD2 in the asymmetric unit. Coot [34] and REFMAC5 [35] were used for building the model and refinement. MOLPROBITY [36] was used for model validation and analysis.

PARP14 MD3
X-ray diffraction data collected for the PARP14 MD3 fragment screen was processed using the Diamond autoprocessing pipeline, utilising *xia2* [37] and *DIALS* [38], and programs from the CCP4 suite [39]. Electron-density maps were generated using the XChemExplorer [40] via DIMPLE [41]. Ligand restraints were generated with AceDRG [42] and ligand binding was detected with PanDDA [43], with ligands built into PanDDA event maps. Iterative refinement and manual model correction was performed using REFMAC5 [35] and Coot [34], respectively.

References

1. B.A. Gibson, W.L. Kraus. (2012) New insights into the molecular and cellular functions of poly(ADP-ribose) and PARPs. *Nature Reviews Molecular Cell Biology* **13**, 411–424.

2. P. Bai. (2015) Biology of Poly(ADP-Ribose) Polymerases: The Factotums of Cell Maintenance. *Molecular Cell* **58** 947–958.

3. S. Goenka, M. Boothby. (2006) Selective potentiation of Stat-dependent gene expression by collaborator of Stat6 (CoaSt6), a transcriptional cofactor. *PNAS*. **103**, 4210–4215.

4. S. Goenka, H.C. Sung, M. Boothby. (2007) Collaborator of Stat6 (CoaSt6)-associated Poly(ADP-ribose) Polymerase Activity Modulates Stat6-dependent Gene Transcription. *Journal of Biological Chemistry* **282,** 18732–18739.

5. P. Mehrotra, J.P. Riley, R. Patel, F. Li, L. Voss, S. Goenka. (2011) PARP-14 Functions as a Transcriptional Switch for Stat6-dependent Gene Activation. *Journal of Biological Chemistry* **286**, 1767–1776.

6. S.H. Cho, S. Goenka, T. Henttinen, P. Gudapati, A. Reinikainen, C.M. Eischen, R. Lahesmaa, M. Boothby. (2009) PARP-14, a member of the B aggressive lymphoma family, transduces survival signals in primary B cells. *Blood* **113,** 2416–2425.

7. S.H. Cho, A.K. Ahn, P. Bhargava, C.-H. Lee, C.M. Eischen, O. McGuinness, M. Boothby. (2011) Glycolytic rate and lymphomagenesis depend on PARP14, an ADP ribosyltransferase of the B aggressive lymphoma (BAL) family. *PNAS* **108**, 15972–15977.

8. A. Barbarulo, V. Iansante, A. Chaidos, K. Naresh, A. Rahemtulla, G. Franzoso, A. Karadimitris, D.O. Haskard, S. Papa, C. Bubici. (2013) Poly(ADP-ribose) polymerase family member 14 (PARP14) is a novel effector of the JNK2-dependent pro-survival signal in multiple myeloma. *Oncogene* **32**, 4231–4242.

9. Human Protein Atlas available from www.proteinatlas.org.

10. M. Uhlén, L. Fagerberg, B.M. Hallström, C. Lindskog, P. Oksvold, A. Mardinoglu, Å. Sivertsson, C. Kampf, E. Sjöstedt, A. Asplund, I. Olsson, K. Edlund, E. Lundberg, S. Navani, C.A.-K. Szigyarto, J. Odeberg, D. Djureinovic, J.O. Takanen, S. Hober, T. Alm, P.-H. Edqvist, H. Berling, H. Tegel, J. Mulder, J. Rockberg, P. Nilsson, J.M. Schwenk, M. Hamsten, K. von Feilitzen, M. Forsberg, L. Persson, F. Johansson, M. Zwahlen, G. von Heijne, J. Nielsen, F. Pontén. (2015) Proteomics. Tissue-based map of the human proteome. *Science* **347**, 1260419.

11. W. Huang, M. Goldfischer, S. Babayeva, Y. Mao, K. Volyanskyy, N. Dimitrova, J.T. Fallon, M. Zhong. (2015) Identification of a novel *PARP14-TFE3* gene fusion from 10-year-old FFPE tissue by RNA-seq. *Genes, Chromosomes Cancer.* **54**, 500–505.

12. P. Mehrotra, A. Hollenbeck, J.P. Riley, L. Fang, R.J. Patel, N. Akhtar, S. Goenka. (2013) PARP-14 and its enzyme activity regulates Th2 differentiation and allergic airway disease. *Journal of Allergy and Clinical Immunology* **131,** 521–531.

13. P. Mehrotra, P. Krishnamurthy, J. Sun, S. Goenka, M.H. Kaplan. (2015) Poly-ADP-ribosyl polymerase-14 promotes T helper 17 and follicular T helper development. *Immunology* **146**, 537–546.

14. A.K.L. Leung, S. Vyas, J.E. Rood, A. Bhutkar, P.A. Sharp, P. Chang. (2011) Poly(ADP-Ribose) Regulates Stress Responses and MicroRNA Activity in the Cytoplasm. *Molecular Cell* **42,** 489–499.

15. R. Zaffini, G. Gotte, M. Menegazzi. (2018) Asthma and poly(ADP-ribose) polymerase inhibition: A new therapeutic approach. *Drug Design, Development and Therapy* **12**, 281–293.

16. P. Krishnamurthy, M.H. Kaplan. (2016) STAT6 and PARP Family Members in the Development of T Cell-dependent Allergic Inflammation. *Immune Network* **16,** 201–210.

17. H. Iwata, C. Goettsch, A. Sharma, P. Ricchiuto, W.W. Bin Goh, A. Halu, I. Yamada, H. Yoshida, T. Hara, M. Wei, N. Inoue, D. Fukuda, A. Mojcher, P.C. Mattson, A.-L. Barabási, M. Boothby, E. Aikawa, S.A. Singh, M. Aikawa. (2016) PARP9 and PARP14 cross-regulate macrophage activation via STAT1 ADP-ribosylation. *Nature Communications* **7**, 1–19.

18. G. Caprara, E. Prosperini, V. Piccolo, G. Sigismondo, A. Melacarne, A. Cuomo, M. Boothby, M. Rescigno, T. Bonaldi, G. Natoli. (2018) PARP14 Controls the Nuclear Accumulation of a Subset of Type I IFN–Inducible Proteins. *Journal of Immunology*, ji1701117.

19. B. Peng, A.G. Thorsell, T. Karlberg, H. Schüler, S.Q. Yao. (2017) Small Molecule Microarray Based Discovery of PARP14 Inhibitors. *Angewandte Chemie - International Edition* **56**, 248–253.

20. K. Upton, M. Meyers, A.-G. Thorsell, T. Karlberg, J. Holechek, R. Lease, G. Schey, E. Wolf, A. Lucente, H. Schüler, D. Ferraris. (2017) Design and synthesis of potent inhibitors of the mono(ADP-ribosyl)transferase, PARP14. *Bioorganic & Medical Chemistry Letters* **27**, 5–9.

21. M. Yoneyama-Hirozane, S. Matsumoto, Y. Toyoda, K.S. Saikatendu, Y. Zama, K. Yonemori, M. Oonishi, T. Ishii, T. Kawamoto. (2017) Identification of PARP14 inhibitors using novel methods for detecting auto-ribosylation. *Biochemical and Biophysical Research Communications* **486,** 626–631.

22. E. Wahlberg, T. Karlberg, E. Kouznetsova, N. Markova, A. Macchiarulo, A.-G. Thorsell, E. Pol, A. Frostell, T. Ekblad, D. Oncu, B. Kull, G.M. Robertson, R. Pellicciari, H. Schuler, J. Weigelt. (2012) Family-wide chemical profiling and structural analysis of PARP and tankyrase inhibitors. *Nature Biotechnology* **30**, 283–288.

23. M. Moustakim, K. Riedel, M. Schuller, A.P. Gehring, O.P. Monteiro, S.P. Martin, O. Fedorov, J. Heer, D.J. Dixon, J.M. Elkins, S. Knapp, F. Bracher, P.E. Brennan. (2018) Discovery of a novel allosteric inhibitor scaffold for polyadenosine-diphosphate-ribose polymerase 14 (PARP14) macrodomain 2. *Bioorganic & Medicinal Chemistry*.

24. A.H. Forst, T. Karlberg, N. Herzog, A.G. Thorsell, A. Gross, K.L.H. Feijs, P. Verheugd, P. Kursula, B. Nijmeijer, E. Kremmer, H. Kleine, A.G. Ladurner, H. Schüler, B. Lüscher. (2013) Recognition of mono-ADP-ribosylated ARTD10 substrates by ARTD8 macrodomains. *Structure* **21**, 462–475.

25. C.M. Nicolae, E.R. Aho, K.N. Choe, D. Constantin, H.J. Hu, D. Lee, K. Myung, G.L. Moldovan. (2015) A novel role for the mono-ADP-ribosyltransferase PARP14/ARTD8 in promoting homologous recombination and protecting against replication stress. *Nucleic Acids Research* **43**, 3143–3153.

26. M. Schuller, K. Riedel, I. Gibbs-Seymour, K. Uth, C. Sieg, A.P. Gehring, I. Ahel, F. Bracher, B.M. Kessler,

J.M. Elkins, S. Knapp. (2017) Discovery of a Selective Allosteric Inhibitor Targeting Macrodomain 2 of Polyadenosine-Diphosphate-Ribose Polymerase 14. *ACS Chemical Biology* **12**, 2866–2874.

27. PerkinElmer, A Practical Guide to working with AlphaScreen, User Guide. (2004). www.perkinelmer.com.

28. M. Philpott, J. Yang, T. Tumber, O. Fedorov, S. Uttarkar, P. Filippakopoulos, S. Picaud, T. Keates, I. Felletar, A. Ciulli, S. Knapp, T.D. Heightman. (2011) Bromodomain-peptide displacement assays for interactome mapping and inhibitor discovery. *Molecular BioSystems* **7**, 2899–2908.

29. R. Tobias, S. Kumaraswamy, Biomolecular Binding Kinetics Assays on the Octet Platform, Appl. Note by fortéBio (Pall Life Sci. (2013)). http://www.biophysics.bioc.cam.ac.uk/wp-content/uploads/2011/02/ForteBio_App_Note_14.pdf.

30. P.M. Collins, T. Ng, R. Talon, K. Nekrosiute, N.M. Pearce, F. Von Delft. (2017) Gentle, fast and effective crystal soaking by acoustic dispensing. *Acta Crystallographica Section D: Structural Biology* **73**, 246–255.

31. A.G.W. Leslie, H.R. Powell. (2007) Processing Diffraction Data with Mosflm. *Evolving Methods for Macromolecular Crystallography* **245**, 41–51.

32. P.R. Evans. (2011) An introduction to data reduction: space-group determination, scaling and intensity statistics. *Acta Crystallographica Section D* **67**, 282–292.

33. A.J. McCoy, R.W. Grosse-Kunstleve, P.D. Adams, M.D. Winn, L.C. Storoni, R.J. Read. (2007) Phaser crystallographic software. *Journal of Applied Crystalography* **40**, 658–674.

34. P. Emsley, B. Lohkamp, W.G. Scott, K. Cowtan. (2010) Features and development of *Coot*. *Acta Crystallographica Section D: Biological Crystallography* **66**, 486–501.

35. G.N. Murshudov, P. Skubák, A.A. Lebedev, N.S. Pannu, R.A. Steiner, R.A. Nicholls, M.D. Winn, F. Long, A.A. Vagin. (2011) *REFMAC*5 for the refinement of macromolecular crystal structures. *Acta Crystallographica Section D: Biological Crystallography* **67**, 355–367.

36. V.B. Chen, W.B. Arendall, J.J. Headd, D.A. Keedy, R.M. Immormino, G.J. Kapral, L.W. Murray, J.S. Richardson, D.C. Richardson. (2010) MolProbity: all-atom structure validation for macromolecular crystallography. *Acta Crystallographica Section D* **66**, 12–21.

37. G. Winter (2010) *xia2*: An Expert System for Macromolecular Crystallography Data Reduction, *Journal of Applied Crystallography* **43**, 186–190.

38. D.G. Waterman, G. Winter, R.J. Gildea, J.M. Parkhurst, A.S. Brewster, N.K. Sauter, G. Evans. (2016) Diffraction-geometry refinement in the DIALS framework. *Acta Crystallographica Section D: Structural Biology* **72**, 558–575.

39. M.D. Winn, C. Charles, K.D. Cowtan, E.J. Dodson, P. Emsley, P.R. Evans, R.M. Keegan, E.B. Krissinel, A.G.W. Leslie, A. McCoy, S.J. McNicholas, G.N. Murshudov, N.S. Pannu, E.A. Potterton, H.R. Powell, R.J. Read, A. Vagin, K.S. Wilson. (2011) Overview of the *CCP*4 suite and current developments. *Acta Crystallographica Section D: Biological Crystallography* **67**, 235–242.

40. T. Krojer, R. Talon, N. Pearce, P. Collins, A. Douangamath, J. Brandao-Neto, A. Dias, B. Marsden, F. Von Delft. (2017) The *XChemExplorer* graphical workflow tool for routine or large-scale protein–ligand structure determination research papers. *Acta Crystallographica Section D: Structural Biology* **73**, 267–278.

41. M. Wojdyr, R. Keegan, G.W. Winter, A. Ashton. DIMPLE - a pipeline for the rapid generation of difference maps from protein crystals with putatively bound ligands. *Acta Crystallographica Section A.* **69**, s299.

42. F. Long, R.A. Nicholls, P. Emsley, S. Grazulis, A. Merkys, A. Vaitkus, G.N. Murshudov. (2017) *AceDRG*: a stereochemical description generator for ligands research papers, *Acta Crystallographica Section D: Structural Biology* **73**, 112–122.

43. N.M. Pearce, T. Krojer, A.R. Bradley, P. Collins, R.P. Nowak, R. Talon, B.D. Marsden, S. Kelm, J. Shi, C.M. Deane, F. Von Delft. (2017) A multi-crystal method for extracting obscured crystallographic states from conventionally uninterpretable electron density. *Nature Communications* **8**, 1–8.

TEP IMPACT

We respectfully request that this document is cited using the DOI value as given above if the content is used in your work.

TEP IMPACT